Science
AAAS

Real-Time Imaging of Pt_3Fe Nanorod Growth in Solution

Hong-Gang Liao *et al.*

Science **336**, 1011 (2012);
DOI: 10.1126/science.1219185

This copy is for your personal, non-commercial use only.

If you wish to distribute this article to others, you can order high-quality copies for your colleagues, clients, or customers by clicking here.

Permission to republish or repurpose articles or portions of articles can be obtained by following the guidelines here.

The following resources related to this article are available online at www.sciencemag.org (this information is current as of October 24, 2014):

Updated information and services, including high-resolution figures, can be found in the online version of this article at:
http://www.sciencemag.org/content/336/6084/1011.full.html

Supporting Online Material can be found at:
http://www.sciencemag.org/content/suppl/2012/05/23/336.6084.1011.DC1.html

A list of selected additional articles on the Science Web sites **related to this article** can be found at:
http://www.sciencemag.org/content/336/6084/1011.full.html#related

This article **cites 36 articles**, 13 of which can be accessed free:
http://www.sciencemag.org/content/336/6084/1011.full.html#ref-list-1

This article has been **cited by** 4 articles hosted by HighWire Press; see:
http://www.sciencemag.org/content/336/6084/1011.full.html#related-urls

This article appears in the following **subject collections:**
Materials Science
http://www.sciencemag.org/cgi/collection/mat_sci

Downloaded from www.sciencemag.org on October 24, 2014

Science (print ISSN 0036-8075; online ISSN 1095-9203) is published weekly, except the last week in December, by the American Association for the Advancement of Science, 1200 New York Avenue NW, Washington, DC 20005. Copyright 2012 by the American Association for the Advancement of Science; all rights reserved. The title *Science* is a registered trademark of AAAS.

Real-Time Imaging of Pt_3Fe Nanorod Growth in Solution

Hong-Gang Liao,[1] Likun Cui,[1] Stephen Whitelam,[1,2] Haimei Zheng[1]*

The growth of colloidal nanocrystal architectures by nanoparticle attachment is frequently reported as an alternative to the conventional growth by monomer attachment. However, the mechanism whereby nanoparticle attachment proceeds microscopically remains unclear. We report real-time transmission electron microscopy (TEM) imaging of the solution growth of Pt_3Fe nanorods from nanoparticle building blocks. Observations revealed growth of winding polycrystalline nanoparticle chains by shape-directed nanoparticle attachment followed by straightening and orientation and shape corrections to yield single-crystal nanorods. Tracking nanoparticle growth trajectories allowed us to distinguish the force fields exerted by single nanoparticles and nanoparticle chains. Such quantification of nanoparticle interaction and understanding the growth pathways are important for the design of hierarchical nanomaterials and controlling nanocrystal self-assembly for functional devices.

Nanocrystals with different shapes and architectures are of considerable interest (*1*–*6*). Uncovering the growth mechanisms responsible for these various architectures has been a topic of intense study. Although nanocrystals have been achieved by a variety of solution growth processes (*1*, *7*–*10*), theories on the growth mechanisms largely fall into one of two categories: growth by monomer attachment or by nanoparticle attachment. According to classical theories of crystal growth, the shape of a nanocrystal is controlled by the relative surface energies of the different crystalline facets, such that higher-energy facets grow faster (*1*, *11*). Growth is assumed to proceed by monomer attachment to the existing nuclei. However, many recent studies suggest that nanoparticles can act as "artificial atoms" and form building blocks for the growth of hierarchical nanostructures. For example, there have been reports of growth by oriented attachment where small nanoparticles interact with each other to form single-crystal lattices (*3*, *7*, *10*, *12*–*14*). Similar growth has been found in the formation of numerous natural crystals by biomineralization processes (*7*, *15*).

Critical questions concerning how nanocrystal architectures grow from nanoparticle building blocks remain unresolved. For instance, it is unclear how the growth process of addition by nanoparticles (instead of monomers) takes place if growth is initiated in a molecular precursor solution. Does the process proceed by nanoparticles attaching one by one to a nucleus, analogous to conventional growth by monomer attachment? Is there a preferred facet or orientation for a nanoparticle to attach to an existing nanoparticle?

Recent developments in transmission electron microscopy (TEM) of imaging through liquids using a liquid environmental cell (*16*–*19*) provide the opportunity to address the above questions. One critical challenge is to maintain the small amount of liquid in the viewing window long enough to allow complete reactions, which is a key to study the growth of colloidal nanocrystals with different shapes and architectures. We overcome this challenge by using an advanced liquid handling technique (*20*) and

[1]Materials Sciences Division, Lawrence Berkeley National Laboratory, Berkeley, CA 94720, USA. [2]The Molecular Foundry, Lawrence Berkeley National Laboratory, Berkeley, CA 94720, USA.

*To whom correspondence should be addressed. E-mail: hmzheng@lbl.gov

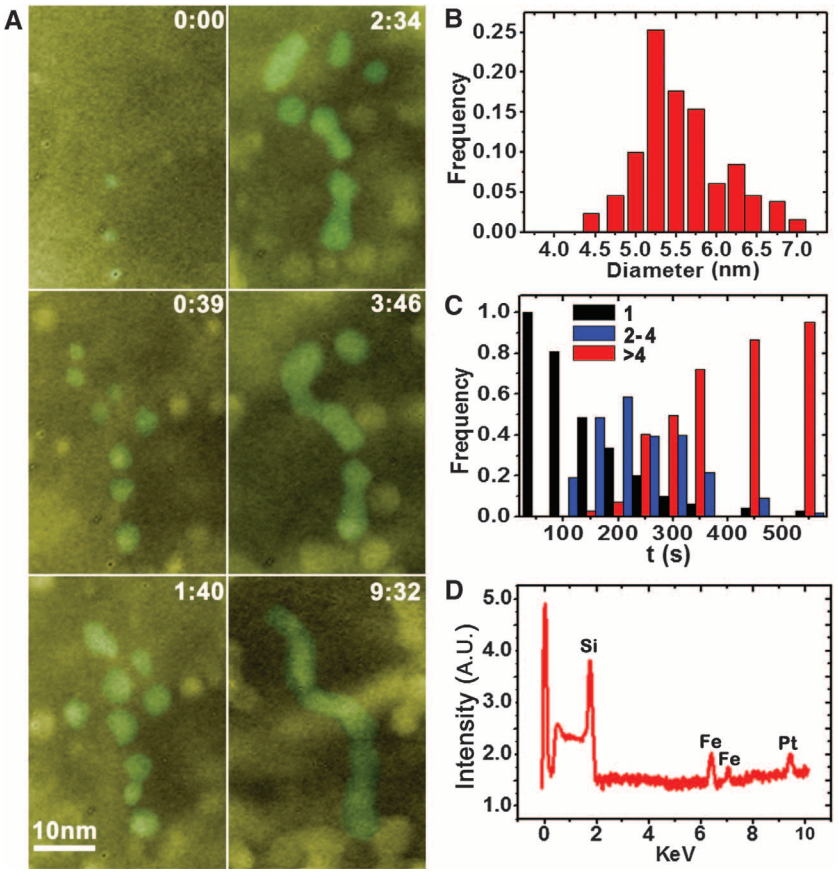

Fig. 1. The growth of Pt_3Fe nanowires in a liquid cell during exposure to the electron beam. A solvent mixture of pentadecane and oleylamine (7:3 vol/vol) was used. (**A**) Sequential color TEM images showing the evolution from the initial nucleation and growth in the molecular precursor solution to a later stage of nanowire formation by shape-directed nanoparticle attachment. Specific nanoparticles that contributed to the nanowire formation are highlighted in green. Time is displayed as minutes:seconds. The initial time is arbitrary. (**B**) Histograms of the particle size distribution when nanoparticle attachment begins. (**C**) Statistics of the length of nanoparticle chain as a function of time. Data are collected in a time window from 1 min 40 s to 9 min 32 s corresponding to (A). (**D**) EDS spectra of Pt_3Fe nanowires obtained ex situ from the same liquid cell. The observed Si signal is from the silicon nitride membrane.

achieve the growth of large–aspect ratio Pt_3Fe nanorods (up to 40:1) by allowing nanoparticles to interact in solution for an extended period of time. We show the real-time imaging of the dynamic growth of Pt_3Fe nanorods by shape-directed nanoparticle attachment.

The growth solution is prepared by dissolving $Pt(acetylacetonate)_2$ (20 mg/ml) and $Fe(acetylacetonate)_2$ (20 mg/ml) in organic solvent. A solvent mixture of pentadecane and oleylamine (7:3 vol/vol) or a mixture of pentadecane, oleylamine, and oleic acid (6:3:1 vol/vol/vol) is used for the comparison of surfactant effects. About 30 pl of growth solution is loaded into one of the reservoirs in a liquid cell. The solution is drawn into the cell by capillary force and forms a liquid layer (120 nm) sandwiched between two silicon nitride membranes (each with a thickness of 13 nm) at the window. The liquid cell is subsequently sealed with epoxy and loaded into the microscope as a standard TEM sample for imaging. A JEOL 3010 TEM operated at 300 kV and a FEI monochromated F20 UT Tecnai operated at 200 kV are used for in situ imaging. A beam current density of 1×10^5 to 8×10^5 A/m^2 is maintained for the study (*20*). However, the intensity can vary briefly at the initial exposure to the electron beam during the time period required to focus for imaging (a few seconds). A CM200 with an energy-dispersive x-ray spectroscopy (EDS) detector is used for elemental analysis following the in situ experiments. An aberration-corrected TEM (TEAM0.5) operated at 300 kV is used for high-angle annular dark field (HAADF) high-resolution scanning TEM (STEM) imaging.

Figure 1A shows sequential images depicting the growth trajectory of a Pt_3Fe nanowire (twisted nanorod) (also see movie S1 for details). Three distinct stages of growth can be identified. During the first stage, many small nanoparticles are formed when the Pt and Fe precursors are reduced by electron beam illumination. Some of them grow by monomer attachment; others undergo coalescence. The nanoparticles merged by coalescence relax into spherical nanoparticles (fig. S1 and movie S1). Eventually, these nanoparticles reach an average size of 5.3 ± 0.9 nm (Fig. 1B). Such growth of monodisperse nanoparticles by parallel monomer attachment and coalescence is similar to the previously observed colloidal Pt nanoparticle growth (*17*). Subsequently, the second stage of growth begins, which is dominated by nanoparticles interacting with each other to form nanoparticle chains. Real-time observation of nanoparticle chain formation by shape-directed nanoparticle attachment and the successive structural relaxation into straight Pt_3Fe nanorods reveals critical mechanisms of the growth of nanocrystal architectures from nanoparticle building blocks. Initially, one nanoparticle meets another, forming a dimer. Unlike in the first stage of growth, the dimer does not relax into a sphere. Instead, a trimer is formed when another particle connects to the dimer end, and additional end-to-end attachments generate a nanoparticle chain. A long nanoparticle chain can also form when short chains of nanoparticles connect to each other. Figure 1C shows the change of chain length as a function of growth time. It is clear that only single nanoparticles exist at the beginning; as growth proceeds, small aggregates (chains of two to four nanoparticles) become dominant. Ultimately, only long chains of nanoparticles are observed. This indicates that not only single nanoparticles but also short nanoparticle chains can be the fundamental building blocks for Pt_3Fe nanowire formation. EDS studies (Fig. 1D) confirm that all the nanocrystals are composed of Pt and Fe with an atomic ratio of roughly 3:1. Further high-resolution TEM (HRTEM) (fig. S1) and electron diffraction studies show a face-centered cubic (fcc) Pt_3Fe crystal structure. Nanocrystals appear with high crystallinity, and a lattice constant of about 0.39 nm (similar to the bulk value) is achieved.

The nanoparticle chains formed during the early stage are winding and markedly flexible. The relative position of the nanoparticles within the chain changes and the orientation of individual nanoparticles also alters, as indicated by the diffraction contrast variations with time (movies S1 to S3). During the final stage of growth, adjacent nanoparticles within the chain contact each other, forming a neck at which, presumably, surfactant molecules are excluded. Subsequently, mass redistribution eliminates the neck, and a smooth nanowire is formed. The diameter of the nanowire is slightly smaller (about 4.0 nm) than that of the individual nanoparticles before attachment (5.3 nm). A bent polycrystalline nanowire can straighten and transform into a single-crystal nanorod with well-defined shape. This final stage of structural relaxation sometimes proceeds in parallel with the second stage of nanoparticle attachment. Notably, most of the nanowires remain twisted and polycrystalline for an extended period of time.

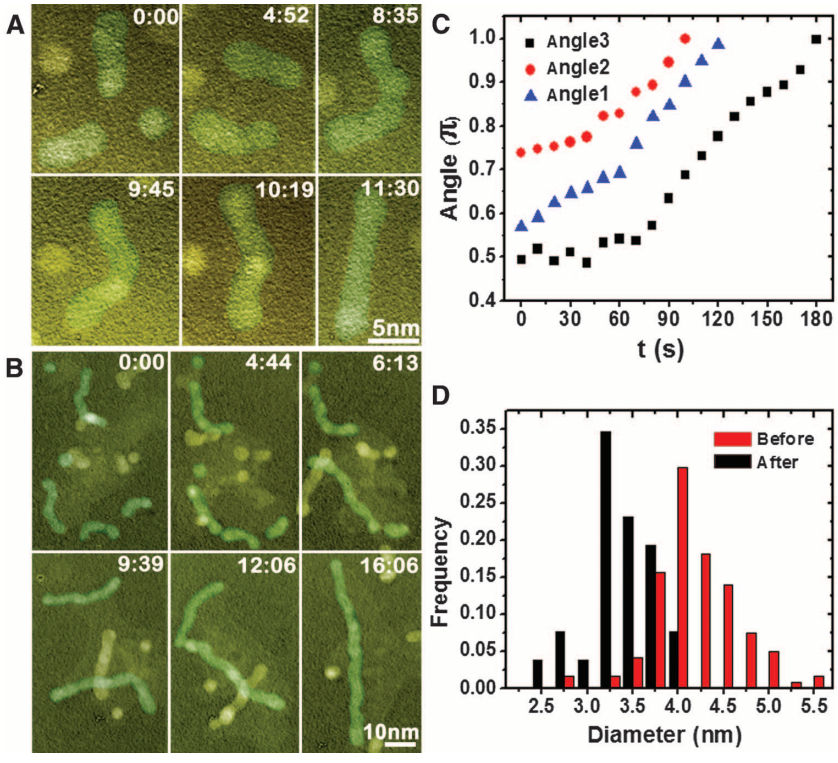

Fig. 2. Formation of twisted Pt_3Fe nanorods and the subsequent straightening process. A solvent mixture of pentadecane, oleylamine, and oleic acid (6:3:1 vol/vol/vol) was used. (**A**) Sequential color TEM images of the growth of a short Pt_3Fe nanorod. (**B**) Sequential color TEM images showing the growth of a long Pt_3Fe nanorod. In both (A) and (B), time is displayed as minutes:seconds. Initial time is arbitrary. Nanorods and the specific particles as building blocks for nanorod formation are highlighted in green. (**C**) The change in contact angle as a function of time after two nanorod building blocks join together. (**D**) Histograms of particle size distribution at the beginning of Pt_3Fe nanorod formation and nanorod diameter distribution after structural relaxation.

Straight nanorods are produced when additional surfactant (10% oleic acid) is added to the growth solution. In this case, the growth solution possesses a solvent mixture of pentadecane, oleylamine, and oleic acid (6:3:1 vol/vol/vol), which differs from that of the above solvent mixture of pentadecane and oleylamine (7:3 vol/vol). First, winding nanoparticle chains are formed following the same growth pathways as shown in Fig. 1A. Chains subsequently straighten and form single-crystal nanorods within a short period of time. Figure 2, A and B, shows the formation of two individual straight nanorods by nanoparticle attachment (also see movies S2 and S3). Nanoparticles or short nanoparticle chains move in liquid by translational and rotational motion. Their preference of adhering to the end instead of the side of a chain strongly suggests the predominance of dipolar forces, as discussed below. Nanorods with different lengths straighten with a similar rate. We measured the change in the contact angle between two short nanorods after they connected as a function of time (Fig. 2C; see images of the three selected nanorods in fig. S2). A higher rate of straightening process is observed at later times when the "neck" between nanoparticles is eliminated. It is likely that different mechanisms are involved in different stages of the straightening process. The slower straightening process at the early stage may arise from the predominance of mass redistribution through the nanoparticle surface to eliminate the neck.

We believe the straightening process is driven by the decrease in total system energy by reducing surface energy and eliminating crystal defects. In the presence of oleic acid, the average diameter of individual nanoparticles at the beginning of nanoparticle chain formation is 4.0 nm (5.3 nm in the absence of oleic acid). The average diameter of a straight nanorod becomes 3.3 nm after structural relaxation (Fig. 2D). The coabsorption of oleylamine and oleic acid on the nanoparticle surface may stabilize the nanoparticles at a smaller size than their counterparts in the absence of oleic acid (*10*, *21*). As the size of the nanoparticle decreases, the higher surface energy arising from the higher surface-to-volume ratio expedites the straightening process. The surfactant effects on the growth of Pt_3Fe nanocrystals have also been observed in our additional experiments. As shown in fig. S3, when surfactant concentration changes drastically, the growth of Pt_3Fe nanocrystals follows a different shape evolution process under the same electron beam conditions. These results demonstrate that the growth is highly influenced by surfactant absorption on the nanocrystal surface and not by TEM imaging mechanisms.

After a nanorod straightens, it takes additional time to form a single-crystal structure. It also takes longer to form a long single-crystal nanorod than a short one. A Pt_3Fe nanorod imaged using HAADF STEM (Fig. 3A) shows that although the rod is straight with a smooth surface, polycrystalline features remain. There are dispersed iron-rich regions in the Pt_3Fe nanorod as well as in individual nanoparticles and dimers, as indicated by the dark spots in the images (examples are marked by arrows in Fig. 3A). The composition nonuniformity across an alloy nanocrystal is commonly observed in flask synthesis (*22*), which agrees with our results. By comparing a Pt_3Fe nanorod with an individual nanoparticle or a dimer, it is clear that the sizes of iron-rich regions are smaller at the later stage as structure relaxation proceeds. This suggests that diffusion and mass redistribution are not limited to the nanocrystal surface during the structural relaxation.

It is notable that a twisted polycrystalline Pt_3Fe nanoparticle chain assembled by imperfect nanoparticle attachment can straighten and correct the orientation to yield a single-crystal nanorod with a perfectly straight shape. We conducted additional in situ studies and obtained snapshot images along the growth trajectory with higher resolution. Figure 3B shows a chain of three connected nanoparticles possessing different orientations from imperfect attachment. Lattice rotation accompanied by mass redistribution and straightening is observed afterward. A single-crystal nanorod is formed shortly after the chain straightens.

To distinguish the force fields exerted by nanoparticles and higher-order structures, we measured the velocity, v, of a spherical nanoparticle as it approached (I) another spherical nanoparticle or (II) a nanoparticle chain. The distance considered is the nearest surface distance between two nanoparticles. We tracked four pairs in either case and used an average chain length of five nanoparticles for case (II) (fig. S4). The average velocity plotted as a function of interparticle distance (Fig. 4A) shows that nanoparticle movements are random when the nanoparticle is above a critical distance from the receiving

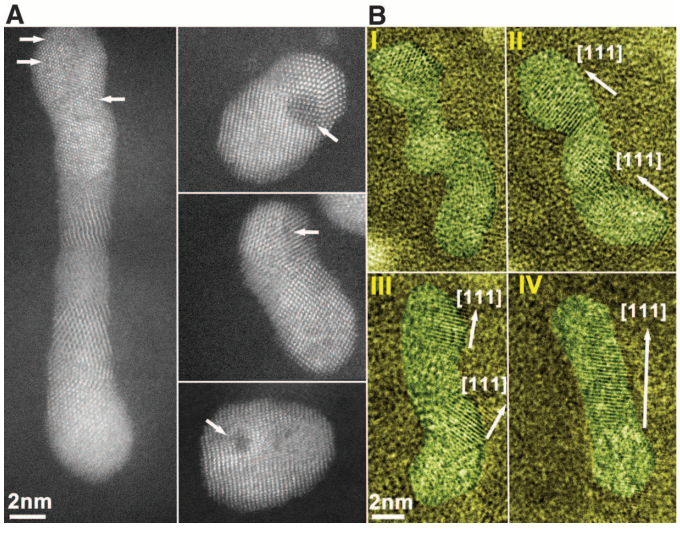

Fig. 3. High-resolution STEM images of Pt_3Fe nanorods and the dynamic shape and orientation changes during structural relaxation. (**A**) HAADF STEM image of a polycrystalline Pt_3Fe nanorod, dimers, and nanoparticles obtained in a liquid cell. The dark spots (examples highlighted by arrows) indicate the iron-rich regions. (**B**) Sequential HRTEM images (I to IV) show both crystal orientation and shape changes during the straightening of a twisted nanoparticle chain. Nanoparticles are highlighted in green.

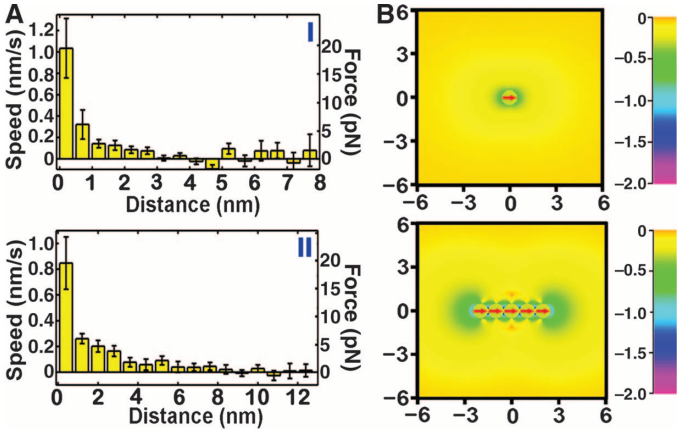

Fig. 4. Nanoparticle interaction as a function of interparticle distance. (**A**) Velocity of a nanoparticle when it approaches (I) another nanoparticle or (II) a nanoparticle chain versus interparticle distance. Error bars show the standard deviation. The right-hand axis shows forces exerted on the approaching nanoparticle. (**B**) Contour maps of the minimum electrostatic interaction energy exerted by a nanoparticle or a nanoparticle chain as a nanoparticle is approaching (a unit of E/k_BT has been used, where k_B is Boltzmann's constant). Each nanoparticle is assumed to be a point electronic dipole. It illustrates that our observation of nanoparticles preferring to attach to the ends of a chain is consistent with dipolar forces mediating nanoparticle attachment.

nanoparticle or nanoparticle chain. As the nanoparticle separation decreases to a critical distance of L_0 = 3 nm when it approaches a spherical nanoparticle or L_0 = ~6 to ~8 nm when it approaches a nanoparticle chain, the nanoparticle acquires a drift velocity, which increases with the decrease in distance. The drift velocity increases greatly at very close approach, indicating the strong attractive forces at short ranges. The right-hand axis of the plot shows the interstructure forces responsible for these drift velocities, calculated assuming the fluctuation dissipation theorem holds (*20*).

Interactions between nanoparticles during the formation of Pt_3Fe nanorods are complex and likely include van der Waals forces, hydrophobic attractions, and charge-charge interactions (*23*–*25*). However, our observation that nanoparticles prefer to attach to nanoparticle chains at their ends, and not in their middle, is strongly suggestive of dipolar interactions (*26*). To illustrate this point, we computed the contour maps of the interaction energy between two nanoparticles and that between a nanoparticle and a nanoparticle chain, assuming each nanoparticle is a distinct point electric dipole. In Fig. 4B, we show the lowest interaction energy of (I) a nanoparticle with another nanoparticle and (II) a nanoparticle with a nanoparticle chain, allowing the approaching nanoparticle to rotate freely. Compared with the interaction potential energy between two nanoparticles (I), the potential energy between a nanoparticle and nanoparticle chain (II) is strongly anisotropic, favoring the end attachment over attachment in the middle of a nanoparticle chain. Previous work has shown that electrostatic dipole moments can be generated by particle faceting (*13*) or surfactants on the nanoparticle surface forming certain patterns (*23*, *27*, *28*). It is also possible that Pt_3Fe nanoparticles possess magnetic dipole moments (*13*, *29*); thus, both electrostatic and magnetic dipole moments may be present in this system [calculation results of magnetic dipolar interaction are similar to those of electrostatic dipolar interaction (*20*)]. However, our experiments show that pure Pt nanorods (unlikely magnetic nanorods) can also grow by nanoparticle attachment following pathways similar to those for Pt_3Fe nanorod formation (fig. S5). These results suggest that the nonmagnetic dipolar interaction (i.e., electrostatic interaction) plays a key role in nanorod growth from nanoparticle building blocks. It also implies that the shape-directed nanoparticle attachment might be an important mechanism for the formation of a variety of one-dimensional nanocrystals.

We have observed the dynamic growth of Pt_3Fe nanorods in solution using TEM. We have identified a range of intricate processes in the growth of nanorods from nanoparticle building blocks, including shape-directed nanoparticle attachment, straightening, orientation correction, and mass redistribution. Visualization of Pt_3Fe nanorod growth trajectories strongly suggests the prominence of dipolar nanoparticle interactions and allows us to quantify the interactions between nanostructures. Understanding the mechanism of one-dimensional colloidal nanocrystal growth using nanoparticles as building blocks provides a link between the world of single molecules and hierarchical nanostructures and paves the way to rational design of nanomaterials with controlled properties.

References and Notes

1. L. Manna, E. C. Scher, A. P. Alivisatos, *J. Am. Chem. Soc.* **122**, 12700 (2000).
2. Y. G. Sun, Y. N. Xia, *Science* **298**, 2176 (2002).
3. C. Pacholski, A. Kornowski, H. Weller, *Angew. Chem. Int. Ed.* **41**, 1188 (2002).
4. D. J. Milliron *et al*., *Nature* **430**, 190 (2004).
5. N. Tian, Z. Y. Zhou, S. G. Sun, Y. Ding, Z. L. Wang, *Science* **316**, 732 (2007).
6. B. Lim *et al*., *Science* **324**, 1302 (2009).
7. J. F. Banfield, S. A. Welch, H. Z. Zhang, T. T. Ebert, R. L. Penn, *Science* **289**, 751 (2000).
8. A. B. Panda, G. Glaspell, M. S. El-Shall, *J. Am. Chem. Soc.* **128**, 2790 (2006).
9. Z. Li *et al*., *Colloids Surf. A Physicochem. Eng. Asp.* **313–314**, 40 (2008).
10. C. Schliehe *et al*., *Science* **329**, 550 (2010).
11. Y. Yin, A. P. Alivisatos, *Nature* **437**, 664 (2005).
12. R. L. Penn, J. F. Banfield, *Science* **281**, 969 (1998).
13. K. S. Cho, D. V. Talapin, W. Gaschler, C. B. Murray, *J. Am. Chem. Soc.* **127**, 7140 (2005).
14. M. Niederberger, H. Cölfen, *Phys. Chem. Chem. Phys.* **8**, 3271 (2006).
15. A. P. Alivisatos, *Science* **289**, 736 (2000).
16. M. J. Williamson, R. M. Tromp, P. M. Vereecken, R. Hull, F. M. Ross, *Nat. Mater.* **2**, 532 (2003).
17. H. M. Zheng *et al*., *Science* **324**, 1309 (2009).
18. J. E. Evans, K. L. Jungjohann, N. D. Browning, I. Arslan, *Nano Lett.* **11**, 2809 (2011).
19. N. de Jonge, F. M. Ross, *Nat. Nanotechnol.* **6**, 695 (2011).
20. Supplementary materials are available on *Science* Online.
21. N. Shukla, C. Liu, P. M. Jones, D. Weller, *J. Magn. Magn. Mater.* **266**, 178 (2003).
22. Y. W. Zhang *et al*., *J. Phys. Chem. C* **112**, 12092 (2008).
23. Y. J. Min, M. Akbulut, K. Kristiansen, Y. Golan, J. Israelachvili, *Nat. Mater.* **7**, 527 (2008).
24. K. J. M. Bishop, C. E. Wilmer, S. Soh, B. A. Grzybowski, *Small* **5**, 1600 (2009).
25. Z. Y. Tang, Z. L. Zhang, Y. Wang, S. C. Glotzer, N. A. Kotov, *Science* **314**, 274 (2006).
26. J. Y. Ku, D. M. Aruguete, A. P. Alivisatos, P. L. Geissler, *J. Am. Chem. Soc.* **133**, 838 (2011).
27. Z. Y. Tang, N. A. Kotov, M. Giersig, *Science* **297**, 237 (2002).
28. K. Liu *et al*., *Science* **329**, 197 (2010).
29. S. H. Sun, C. B. Murray, D. Weller, L. Folks, A. Moser, *Science* **287**, 1989 (2000).

Acknowledgments: We thank P. Geissler (University of California, Berkeley) for helpful discussions. We are also grateful to the comments of B. Sadtler and G. Reinhard. This work was performed using the facility at National Center for Electron Microscopy (NCEM), Lawrence Berkeley National Laboratory (LBNL), and portions of this work were performed at the Molecular Foundry (MF), LBNL. NCEM and MF were supported by the Office of Science, Office of Basic Energy Sciences (BES), Scientific User Facilities Division of the U.S. Department of Energy (DOE) under contract no. DE-AC02-05CH11231. This project was supported by the Office of Basic Energy Sciences, Division of Materials Sciences and Engineering, of the U.S. DOE under contract no. DE-AC02-05CH11231. H.-G.L. thanks J. Park for help on the initial experimental setup. H.Z. thanks the U.S. DOE Office of Science Early Career Research Program for support and gratefully acknowledges partial funding support from LDRD LBNL.

Supplementary Materials

www.sciencemag.org/cgi/content/full/336/6084/1011/DC1
Materials and Methods
Figs. S1 to S10
References (*30*–*39*)
Movies S1 to S3

16 January 2012; accepted 10 April 2012
10.1126/science.1219185

Direction-Specific Interactions Control Crystal Growth by Oriented Attachment

Dongsheng Li,[1] Michael H. Nielsen,[1,2] Jonathan R. I. Lee,[3] Cathrine Frandsen,[4] Jillian F. Banfield,[5,6] James J. De Yoreo[1,7]*

The oriented attachment of molecular clusters and nanoparticles in solution is now recognized as an important mechanism of crystal growth in many materials, yet the alignment process and attachment mechanism have not been established. We performed high-resolution transmission electron microscopy using a fluid cell to directly observe oriented attachment of iron oxyhydroxide nanoparticles. The particles undergo continuous rotation and interaction until they find a perfect lattice match. A sudden jump to contact then occurs over less than 1 nanometer, followed by lateral atom-by-atom addition initiated at the contact point. Interface elimination proceeds at a rate consistent with the curvature dependence of the Gibbs free energy. Measured translational and rotational accelerations show that strong, highly direction-specific interactions drive crystal growth via oriented attachment.

The growth of crystals through the aggregation and coalescence of nanoparticles is now recognized as a widespread phenomenon in biomineral (*1*, *2*), biomimetic (*3*, *4*), and natural systems (*5*) and during the synthetic production of nanoparticles and nanowires (*6*–*8*).